RESEARCH ARTICLE

Efficient triple-layer photoanode incorporated with nitrogen-doped TiO_2 nanocrystals for CdS quantum dot-sensitized solar cells

W.I. Sandamali, G.K.R. Senadeera, T.S.M. Liyanage, J.M.K.W. Kumari, T. Jaseetharan, A.M.J.S. Weerasinghe, V.P.S. Perera, J.C.N. Rajendra, N. Karthikeyan and M.A.K.L. Dissanayake

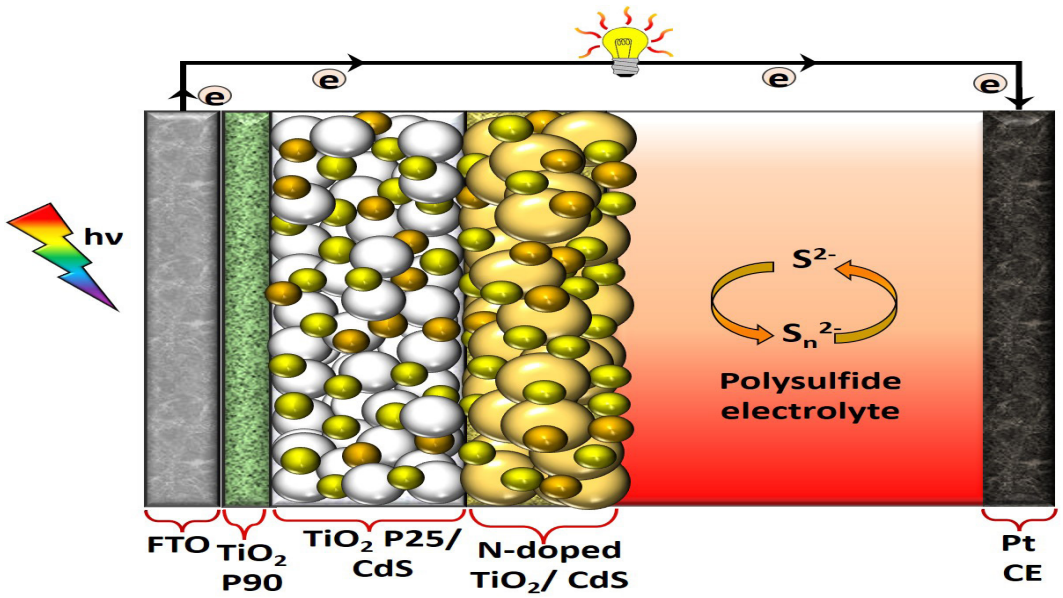

Highlights

- Nitrogen-doped TiO_2 nanocrystals were synthesized by hydrolyzing TTIP with aqueous ammonia.
- Triple layer photoanode consisting of TiO_2 compact layer, mesoporous TiO_2 P25 and nitrogen-doped TiO_2 increased photocurrent generation in CdS QDSSCs.
- Replacing mesoporous TiO_2 P25 layer in the triple-layer photoanode by nitrogen-doped TiO_2 enhanced overall power conversion efficiency of CdS QDSSCs by 29.81 %.

Ceylon Journal of Science 51(4) 2022: 449-457
DOI: http://doi.org/10.4038/cjs.v51i4.8062

RESEARCH ARTICLE

Efficient triple-layer photoanode incorporated with nitrogen-doped TiO_2 nanocrystals for CdS quantum dot-sensitized solar cells

W.I. Sandamali[1,2,*], G.K.R. Senadeera[1, 2], T.S.M. Liyanage[2], J.M.K.W. Kumari[2], T. Jaseetharan[3], A.M.J.S. Weerasinghe[4], V.P.S. Perera[1], J.C.N. Rajendra[1], N. Karthikeyan[1] and M.A.K.L. Dissanayake[2]

[1]*Department of Physics, The Open University of Sri Lanka, Nawala, Nugegoda, Sri Lanka*
[2]*National Institute of Fundamental Studies, Kandy, Sri Lanka*
[3]*Department of Physical Sciences, Faculty of Applied Sciences, South Eastern University of Sri Lanka, Sammanthurai 32200, Sri Lanka*
[4]*School of Chemistry and Physics, Queensland University of Technology, Brisbane 4000, Queensland, Australia*

Received: 30/03/2022; Accepted:11/11/2022

Abstract: Nitrogen-doped (N-doped) TiO_2 nanocrystals were synthesized by adopting a wet chemical method, in which titanium tetraisopropoxide (TTIP) was hydrolyzed with aqueous ammonia under a continuous flow of nitrogen gas. Triple layer photoanode, consisting of TiO_2 P90, TiO_2 P25 and N-doped TiO_2 nanomaterials, was developed by utilizing the spin coating and doctor blading techniques and subjecting to thermal treatment. Photoanodes were sensitized with CdS quantum dots by the successive ionic layer adsorption and reaction method. Quantum dot-sensitized solar cells (QDSSCs) were fabricated by assembling photoanodes with Pt counter electrode and polysulfide electrolyte. Material characterizations for N-doped TiO_2 were conducted by TEM, XRD, UV-Visible spectroscopy and Mott-Schottky techniques. Fabricated QDSSCs were evaluated by incident photon-to-electron conversion efficiency (IPCE) spectroscopy, current-voltage (*J-V*) characteristics and electrochemical impedance spectroscopic (EIS) measurements. QDSSCs with N-doped TiO_2 achieved an overall power conversion efficiency of 1.35 % while QDSSCs with TiO_2 P25 showed only 1.04 %. Overall power conversion efficiency enhancement of 29.81 % was achieved by incorporating N-doped TiO_2 in the triple-layer photoanode, which Is attributed to increased photocurrent generation in the photoanode. Enhanced IPCE and reduced charge transfer resistance at the photoanode/electrolyte interface (R_2ct) agree with improved photoactivity of the triple-layer photoanode incorporated with N-doped TiO_2.

Keywords: N-doped TiO_2, Triple layer TiO_2 photoanode, QDSSC, CdS quantum dots.

INTRODUCTION

Quantum dot-sensitized solar cells (QDSSCs) are advancing to achieve new heights in the third generation of solar cells by exploiting unique characteristics of quantum dots, such as, tunable bandgaps, multiple exciton generation and large extinction coefficient. Conventional QDSSCs are composed of three main components; photoanode, counter electrode, and electrolyte. Photoanodes are fabricated by decorating mesoporous wide bandgap semiconductors; e.g. TiO_2, SnO_2, ZnO etc., with photon capturing quantum dots; e.g. CdS, PbS, CdSe etc. Wide bandgap semiconductors are responsible for providing transport pathways for the photogenerated electrons from quantum dots. Metal chalcogenides and Pt are popular choices for counter-electrode materials. Polysulfide electrolyte is frequently used with QDSSCs as the redox mediator responsible for quantum dot regeneration and hole transportation. As a primary component of QDSSC, photoanode modifications hold a significant place among numerous studies, targeting for increased performance and higher stability. These modifications can be either material-wise or structural-wise. Conventional photoanode consists of a single-layer TiO_2 mesoporous film over a compact layer, which provides sites for quantum dot attachment. TiO_2 is a highly attractive semiconductor material due to low cost, nontoxicity, biocompatibility and abundance in nature. Several groups have attempted to improve inherent properties of TiO_2 by doping with metallic and non-metallic elements, where metal elements were reported to increase thermal instability and recombination (Dissanayake *et al*., 2017; Qiu and Burda, 2007). In relation to dye-sensitized solar cells (DSSCs), replacing TiO_2 photoanode material with N-doped TiO_2 has been investigated by several study groups. Dissanayake et al. reported 89 % of significant efficiency enhancement in DSSCs by utilizing a multilayered photoelectrode with N-doped TiO_2 compared to that of undoped TiO_2 (Dissanayake *et al*., 2017). Furthermore, efficiency enhancement due to favorable traits such as reduction of charge transfer resistance, increased visible light absorption and retarded charge transfer resistance were reported with N-doped TiO_2 photoanodes (Guo *et al*., 2011; Kushwaha *et al*., 2015; Kusumawardani and Narsito, 2010; Tian *et al*., 2010; Z. L. Zhang *et al*., 2017). Similar results were reported with QDSSCs when replacing single-layer TiO_2 photoanode with N-doped TiO_2. Shu et al. reported the photovoltaic performance of CdSe quantum dot-sensitized solar cell (QDSSC) based on mesoscopic nitrogen-doped TiO_2 spheres prepared by solvothermal method and Kumar et al. reported that mild doping of nitrogen passivates surface

**Corresponding Author's Email:* ishara.we@nifs.ac.lk
https://orcid.org/0000-0002-2072-9902

defects in TiO_2 reducing recombination centers (Kumar *et al*., 2020; Shu *et al*., 2012). Furthermore, López-Luke et al. reported the utilization of N-doped TiO_2 nanoparticle thin films produced by a sol-gel method for CdSe QDSSCs (López-Luke *et al*., 2008). However, application of a layer-by-layer structure of N-doped TiO_2 and commercial TiO_2 P25 for photoanodes in quantum dot-sensitized solar cells was not reported previously. Therefore, in order to explore the possibility of using a novel structurally modified photoanode for CdS QDSSCs, in this study we have modified the conventional photoanode structurally by introducing a layer of N-doped TiO_2 on top of a mesoporous TiO_2 P25 layer and investigated the solar cell performances by comparing with devices with conventional TiO_2 P25 photoanodes.

MATERIALS AND METHODS

Materials

Fluorine doped tin oxide (FTO) coated glass (7 Ω cm^{-2}, Solaronix), titanium tetraisopropoxide (97%, Fluka), titanium dioxide P90 powder (Evonik), titanium dioxide powder P25 (Degussa), Triton X-100 (Sigma Aldrich), glacial acetic acid (99%, Fisher), sulfur (99%, Daejng), sodium sulfide hydrate (> 60%, Sigma Aldrich), cadmium (II) chloride (99.99%, Sigma Aldrich), potassium chloride (99%, Aldrich), polyethylene glycol (99.8%, Sigma Aldrich), methanol (99.8%, Sigma Aldrich), and aqueous ammonia (35%, Fluka) were used as received without any modification.

Synthesis of N-doped TiO_2 powder

N-doped TiO_2 was synthesized by a modified wet chemical method, where titanium tetraisopropoxide (TTIP) was hydrolyzed with aqueous ammonia (NH_4OH) (Dissanayake *et al.,* 2017; Guo, Shen, Wu, *et al*., 2011). TTIP (25 ml) was added dropwise to a mixture of NH_4OH (50 ml) and deionized water (100 ml), placed in an ice bath, under vigorous stirring and continuous flow of N_2 gas. The resulting white precipitate was washed several times with deionized water and dried at 80 °C for 1 h. Finally, the powder was sintered at 450 °C for 4 h to obtain yellow-colored N-doped TiO_2.

Fabrication of triple-layered photoanode

Prior to developing the TiO_2 double-layered structure, a compact layer was applied over well cleaned FTO glass substrate, by spin coating a paste of TiO_2 P90 (0.25 g) mixed with diluted HNO_3 (1 ml) followed by sintering at 450 °C for 45 min. As decided from preliminary studies, the TiO_2 double layer structure was prepared by fabricating a TiO_2 P25 layer over the TiO_2 P90 compact layer and fabricating an N-doped TiO_2 layer over the TiO_2 P25 layer, considering the adherence properties and photovoltaic performance of photoanodes. First mesoporous layer was fabricated by the doctor blading a paste of TiO_2 P25 (0.25 g), diluted HNO_3 (1 ml), triton-X 100 (0.05 ml), and polyethylene glycol (0.05 ml) on top of TiO_2 P90 followed by sintering at 450 °C for 45 min. Another TiO_2 layer was fabricated by the doctor blading a paste prepared with N-doped TiO_2 (0.25 g), diluted HNO_3 (1 ml), triton-X 100 (0.05 ml), and polyethylene glycol (0.05 ml) over TiO_2 P25, followed by sintering at 450 °C for 45 min. Fabricated photoanodes were sensitized with CdS quantum dots by successive ionic layer adsorption and reaction (SILAR) technique, using 0.1 M $CdCl_2$ and 0.1 M Na_2S as precursor solutions (Dissanayake *et al*., 2020). Finally, photoanodes were dried at 100 °C.

Device fabrication

Fabricated photo anodes with an active surface area of 0.16 cm^2 were clipped together with a Pt counter electrode. A liquid polysulfide electrolyte layer, composed of sulphur (2 M), Na_2S (0.5 M), and KCl (0.2 M) dissolved in a mixture of deionized water and methanol in the ratio of 3:7 (v/v), was injected in-between to obtain the final QDSSCs.

Characterization techniques

The cross-sectional view of the photoanode was examined by means of Scanning Electron Microscope (SEM) from ZEISS EVO. High resolution transmission electron microscopy (HRTEM) images of N-doped TiO_2 were obtained from AJEOL 2100 TEM. Powder X-ray diffraction (XRD) data of N-doped TiO_2 material was recorded using BrukerD8 advanced eco X-ray diffraction system with Cu Kα radiation (λ = 1.54060 Å), Mott-Schottky measurements were taken by using a three-electrode setup composed of Pt wire CE, Ag/AgCl standard reference electrode, and fabricated photoanode as the working electrode, with a Metrohm Autolab (PGSTAT128 N) potentiostat/ galvanostat, at a frequency of 1.0 kHz. Optical absorption spectra of different materials were recorded by Shimadzu 2450 UV-Vis spectrophotometer. The incident photon-to-current conversion efficiency (IPCE) measurements were taken for fabricated QDSSCs, by using a Bentham PVE 300 unit with a TMC 300 monochromator-based IPCE system with a 150 W Xenon arc lamp. Current density-voltage (*J-V*) characterizations and electrochemical impedance spectroscopy (EIS) measurements of fabricated QDSSCs were carried out under simulated light of 100 mW cm^{-2} with AM 1.5 filter by coupling an Oriel Newport LCS-100 solar illumination system with a Metrohm Autolab potentiostat/ galvanostat, combined with an FRA 32 M Frequency Response Analyzer (FRA) covering the frequency range between 1 MHz and 0.01 Hz.

RESULTS AND DISCUSSION

Morphological characterization

Figure 1 shows photographs of samples of (a) commercial TiO_2 P25, and (b) synthesized N-doped TiO_2 respectively, where apparent color changes from white to yellow was observed compared to TiO_2 P25, indicating deviated interaction with visible light.

Figure 2. (a) displays a cross-sectional SEM image of the fabricated TiO_2 P25/ N-doped TiO_2 photoanode. A very thin layer of TiO_2 P90 (~ 0.9 µm) was observed over FTO glass substrate and a layer TiO_2 P25 of about 6.8 µm thickness was observed on top of the TiO_2 P90 layer. The top most layer was composed of N-doped TiO_2 (~ 11.5 µm) and appears to be more porous in nature compared

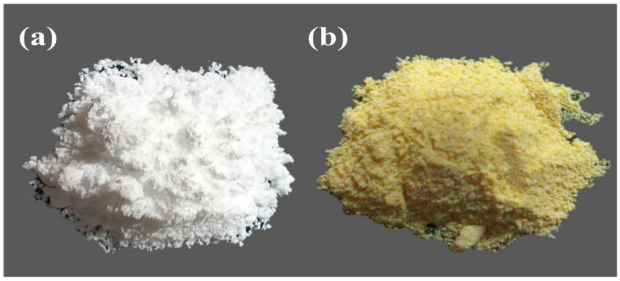

Figure 1: (a) Degussa TiO_2 P25 and (b) N-doped TiO_2.

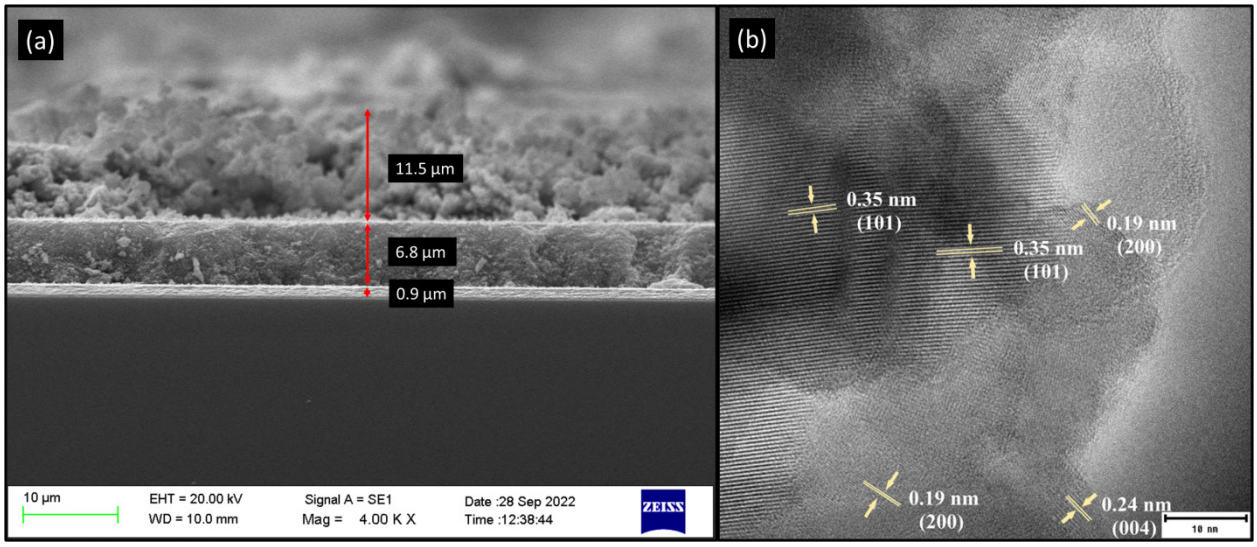

Figure 2: (a) Cross-section SEM image of the TiO_2 P25/ N-doped TiO_2 photoanode and (b) HRTEM image of N-doped TiO_2 .

to the TiO_2 P25 film. In addition, Figure 2. (b) shows a HRTEM image of prepared N-doped TiO_2, which was sintered at 450 °C for 4 h. Lattice fringes were observed due to diffractions from the N-doped TiO_2 crystal structure. Measured interplanar (d) spacing values of 0.35 nm, 0.24 nm and 0.19 nm, in-between these fringes correspond to (101), (004) and (200) lattice planes of tetragonal anatase TiO_2 crystals.

XRD analysis

Powder X-ray diffraction (XRD) patterns were obtained for the identification of crystallization and phase orientation of TiO_2 samples. Figure 3 displays obtained XRD data of prepared N-doped TiO_2 material sintered at 450 °C for 4 h, compared with commercial TiO_2 P25 powder. XRD peaks of TiO_2 P25 observed at 25.30°, 37.04°, 37.82°, 38.57°, 48.01°, and 54.07° angular positions correspond to (101), (103), (004), (112), (200), and (105) planes of TiO_2 anatase crystal structure, while XRD peaks observed at 27.45°, 36.04°, and 41.43° angular positions corresponds to (110), (101), and (111) planes of TiO_2 rutile crystal structure (Baur & Khan, 1971; Horn *et al*., 1972). The percentage of anatase in the TiO_2 P25 sample was calculated to be 82.5 %, using the following equation,

$$A\,\% = \frac{100}{\left[1 + 1.265\left(\frac{I_R}{I_A}\right)\right]} \quad (1)$$

where, I_R is the integrated intensity of the rutile peak at 27.45° (110) and I_A is the integrated intensity of the anatase peak at 25.30° (101) (Spurr & Myers, 1957; Tayade *et al.,* 2018)According to Figure 3, observed XRD peaks of N-doped TiO_2 material correspond to (101), (004), (112), (200), and (105) planes of TiO_2 anatase crystal structure, where peaks belonging to TiO_2 rutile crystal structure were found to be absent. The average crystallite size of the anatase TiO_2 crystals in both samples were estimated from the XRD peak at 25.30° corresponding to (101) crystal plane using the following Scherrer equation,

$$D = \frac{k\lambda}{\beta_{hkl}.\cos\theta_{hkl}} \quad (2)$$

where, D is the average crystallite size, λ is the wavelength of X-ray (Cu Kα1 - 0.154060 nm), k is the shape factor (0.94), β_{hkl} is the full width half maximum (FWHM) of the diffraction peak, and θ_{hkl} is the Bragg angle (Murugan, 2015; Scherrer, 1918). Average crystallite size was estimated as 17.20 nm for TiO_2 P25 and 18.67 nm for N-doped TiO_2. Even though, significant peak shifts of N-doped TiO_2, compared to the angular positions of TiO_2 P25 XRD peaks, were not observed, the average crystallite size of N-doped

TiO_2 was increased, which could be attributed to doping of larger atomic radius nitrogen into oxygen (Khan *et al*., 2021).

UV-Visible absorption and Mott-Schottky analysis

In order to understand the interactions of light with different materials employed in the QDSSCs, UV-Visible spectra were obtained using diffuse reflectance of powdered samples. Reflectance data were reconstructed using the following Kubelka-Munk function to obtain the absorbance of related materials

$$F(R_\infty) = \frac{(1-R_\infty)^2}{2R_\infty} = \frac{K}{S} \quad (3)$$

where, $F(R_\infty)$ is the Kubelka-Munk function corresponding to absorbance, R_∞ is the absolute reflectance, K is the absorption coefficient, and S is the scattering coefficient (Kubelka and Munk, 1931; Patil *et al*., 2013). As evident from Figure 4, both TiO_2 P25 and N-doped TiO_2 show a strong absorption in the UV region ($\lambda < 400$ nm). However, when both of these samples are compared, only N-doped TiO_2 indicates notable light activity in the visible region. CdS, as the sensitizer employed for photocurrent generation in the QDSSC, absorbs light photons in the range of 400-550 nm. Photoanode material in the optimized device included with N-doped TiO_2 shows excessive absorption in the visible region compared to the device with TiO_2 P25.

Optical bandgap values of TiO_2 P25 and N-doped TiO_2 were calculated by adopting Tauc equation for indirect bandgap materials as mentioned below,

$$[F(R_\infty)h\nu]^{1/2} = A\,(h\nu - Eg) \quad (4)$$

where, $F(R_\infty)$ is the Kubelka- Munk function, R_∞ is the absolute reflectance, h is the Planck's constant, $h\nu$ is the photon energy, A is the proportional constant, and Eg is the optical bandgap (Abeles, 1972; Patil *et al*., 2013). Figure 5. (a) presents extrapolated slopes of Tauc plots, where a negative shift in bandgap was observed with N-doped TiO_2 (3.00 eV) compared to TiO_2 P25 (3.14 eV). Past studies suggest that, when nitrogen atoms occupy oxygen sites in the TiO_2 lattice, narrowing of the energy bandgap occurs resulting in a red-shifted absorbance (Khan *et al*., 2021; Kusumawardani and Narsito, 2010; J. Zhang *et al*., 2011). In order to understand the energetics of semiconductor (SC) photoanode/ electrolyte junction, Mott-Schottky plots were obtained under the constant frequency of 1 kHz in 0.1 M aqueous Na_2SO_4 electrolyte. As displayed in Figure. 5 (b) Mott-Schottky plots for both TiO_2 P25 and TiO_2 P25/ N-doped TiO_2 photoanodes reflect n-type nature of the semiconductors with a positive slope. At the n-type SC/ electrolyte interface, equilibrium will be achieved by transferring electrons from Fermi energy level of SC situated in an upper level to that of the electrolyte. This induces positive charges on the SC, which are effectively counterbalanced with sheet of charge from electrolyte. By artificially changing the voltage in the junction, original band bending to achieve equilibrium of Fermi levels are changed, and flat band potential (V_{fb}) is recorded as the applied voltage when there is no band bending (Gelderman *et al*., 2007; La Mantia *et al*., 2010).

V_{fb} can be estimated from the x intercept of the linear portion of the curve obtained by the graphical representation of the following Mott-Schottky equation,

$$\frac{1}{C^2} = \frac{2}{\varepsilon\varepsilon_0 A^2 e N_D}\left(V - V_{fb} - \frac{k_B T}{e}\right) \quad (5)$$

where, C is the interfacial capacitance, A is the area, N_D is the number of donors, V is the applied voltage, k_B is the Boltzmann's constant, T is the absolute temperature, ε is the dielectric constant of the semiconductor, ε_0 is the permittivity of free space and e is the electronic charge

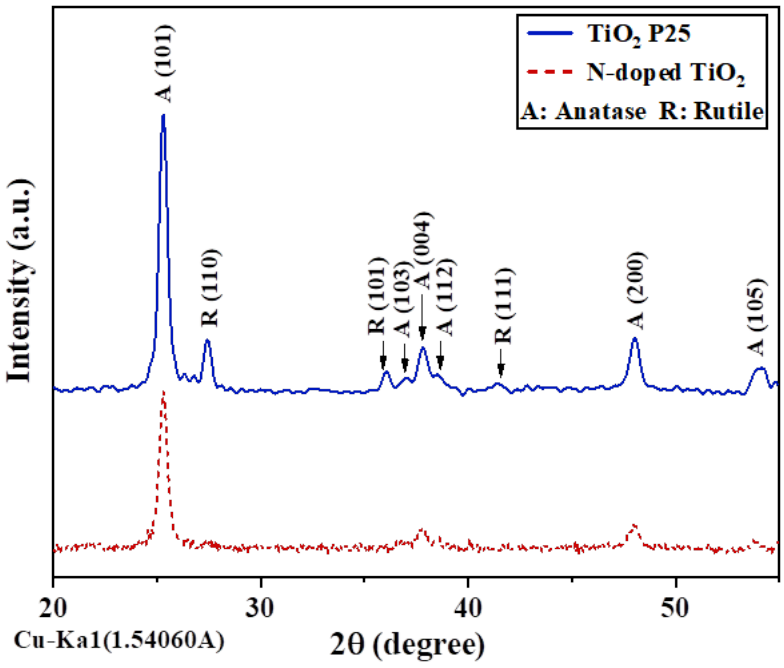

Figure 3: Powder XRD spectrum of N-doped TiO_2

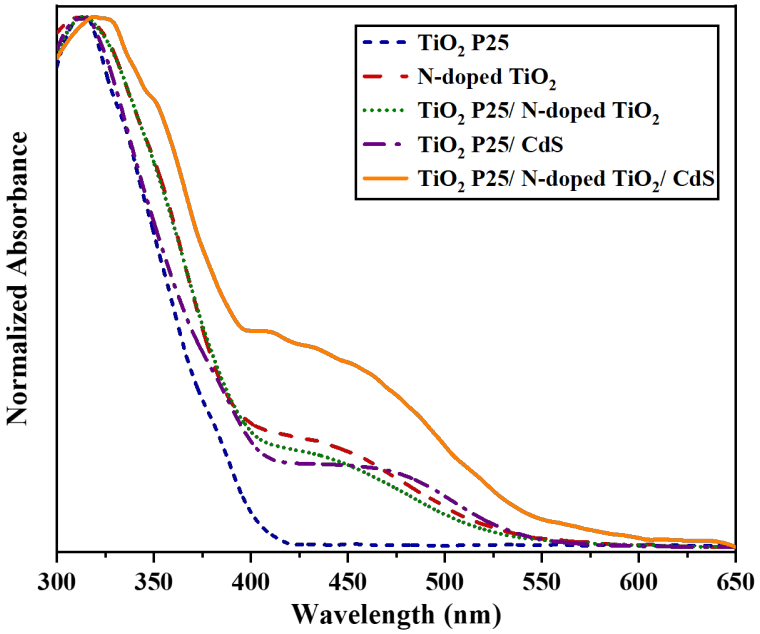

Figure 4: UV-Visible absorption spectra of semiconductors (TiO_2 P25, N-doped TiO_2, TiO_2 P25/ N-doped TiO_2, TiO_2 P25/ CdS, and TiO_2 P25/ N-doped TiO_2/ CdS).

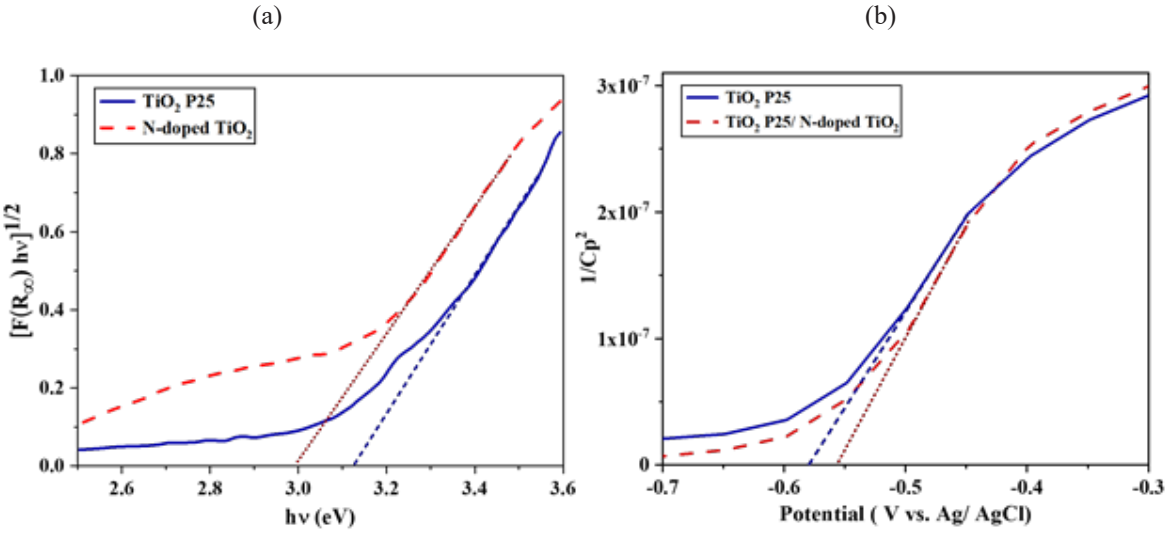

Figure 5: (a) Tauc plot of TiO_2 P25 and N-doped TiO_2 and (b) Mott-Schottky plot of TiO_2 P25 and TiO_2 P25/ N-doped TiO_2 photoanodes.

(Gelderman *et al*., 2007; SATO, 1990).

V_{fb} values of two photoanodes, TiO_2 P25 and TiO_2 P25/ N-doped TiO_2 were estimated to be -0.579 V and - 0.557 V, as shown from the Mott-Schottky plot of $1/C^2$ vs applied voltage in Figure 5. (b), where a slight positive shift was originated in V_{fb} with introduction of the N-doped TiO_2 layer. This was attributed to anodic shift of the conduction band and reduction in band bending which results from altered surface states and oxygen vacancies due to nitrogen doping (Garlisi *et al*., 2018).

Photovoltaic Performance and IPCE Analysis

The current density-voltage (*J-V*) characteristics of QDSSCs were investigated under light irradiation of 100 mW cm^{-2}, to understand the effectiveness of the developed triple-layer photoanode. Figure 6. (a) displays the current density variation of a S_1 QDSSC and a S_2 QDSSC with respect to the voltage of the device. Furthermore, mean and standard deviation values acquired by using photovoltaic parameters of five samples under each of S_1 and S_2 QDSSC categories are presented in Table 1. S_1 QDSSC includes a triple-layer photoanode composed of TiO_2 P90 compact layer, and dual TiO_2 P25 layers, while the photoanode of S_2 QDSSC was fabricated by replacing topmost TiO_2 P25 layer by N-doped TiO_2. As evident from the recorded data, replacement of TiO_2 P25 layer by N-doped TiO_2 layer influenced the increment of power conversion efficiency of QDSSC by 29.81 %, from 1.04 to 1.35 %. Open circuit voltage (*V*oc) of the QDSSC has been slightly reduced by 3.52 % from 435.0 to 420.2 mV when replacing TiO_2 P25

layer with N-doped TiO_2. This trend agrees with the Mott-Schottky plot presented in Figure 5. (b), where a positive shift in Fermi level of new photoanode was suggested due to surface states and oxygen vacancies originated from N-doping. The short circuit current density of S_2 solar cell device was improved from 6.81 to 8.61 mA cm^{-2}, with an increment of 26.43 % compared to the S_1 device. This can be attributed to increased photocurrent generation by CdS quantum dots due to high light scattering in the TiO_2 P25/ N-doped TiO_2 photoanode. Moreover, the porous nature of the photoanode facilitates for fast quantum dot regeneration by effective diffusion of electrolyte and higher amount of quantum dot loading. The fill factor of the S_2 QDSSC was also improved compared to S_1 QDSSC.

The spectral response of fabricated QDSSCs were investigated using the incident photon-to-current conversion efficiency (IPCE) spectra, where the number of photogenerated electrons per incident photon, at a given wavelength is graphically expressed. IPCE at different wavelengths can be calculated using the following

$$IPCE\ \% = \frac{(1240 \times Jsc)}{(\lambda \times I_i)} \times 100 \quad (6)$$

where, *J*sc is the short circuit current density, λ is the excitation wavelength and I_i is the incident light power (Li *et al*., 2014; López-Luke *et al*., 2008). According to the spectra displayed in Figure 6. (b), maximum IPCE peak values of 73 % and 84 % were observed with S_1 and S_2 QDSSCs, at a wavelength of 464 nm, indicating the highest incident photon response of CdS quantum dots. These absorption characteristics observed from IPCE and UV-Visible absorption (Figure 4) spectra correspond to CdS quantum dots with an average diameter of 6 nm, as reported in the literature (Borovaya *et al*., 2014). Moreover, respective integrated current density values of S_1 and S_2 devices were calculated to be 6.04 to 7.11 mA cm^{-2} according to IPCE data obtained (Table 1). As expressed in the spectra, the overall photo activity of the QDSSC has improved with the incorporation of N-doped TiO_2 layer, which is consistent with short circuit current density values discussed previously (Shu *et al*., 2011).

EIS Characterization

Electrochemical impedance spectroscopy (EIS) analysis was conducted for fabricated QDSSCs, under light irradiation of 100 mW cm^{-2}, in order to understand the interfacial charge transfer characteristics inside the solar cells. Impedance data were collected for S_1 and S_2 QDSSCs and obtained Nyquist plots were fitted with equivalent electrical circuit models using NOVA software, as displayed in Figure 7. Two overlapping semicircles were observed in both Nyquist plots. Redox impedance at the electrolyte/ CE interface induces a smaller semicircle in the high-frequency region, while impedance at the photoanode/ electrolyte interface induces a larger semicircle in the mid-frequency region. Symbols in the equivalent circuit represent, the series resistance (*R*s), charge transfer resistance (R_1ct) and chemical capacitance (CPE_1) at the electrolyte/ CE interface, and, charge transfer resistance (R_2ct) and chemical capacitance (CPE_2) at the photoanode/ electrolyte interface (Dissanayake *et al.,* 2021a and 2021b; Li *et al*., 2020). According to the estimated EIS parameters mentioned in Table 2, S_2 QDSSC show slightly improved *R*s due to increased photogenerated electrons flowing in the system. R_2ct of S_2 device showed 25.7% of significant reduction, with resistances changing from 129.0 Ω to 95.8 Ω compared to S_1 device. This can be attributed to improved charge transfer kinetics at the N-doped TiO_2/ polysulfide electrolyte interface due to efficient photocurrent generation in the photoanode (Umair *et al*., 2021). Altered surface states and oxygen vacancies introduced to TiO_2 due to nitrogen doping, as suggested from Mott-Schottky studies (Figure 5. (b)) act as electron-hole recombination centers. This increases the carrier recombination rate

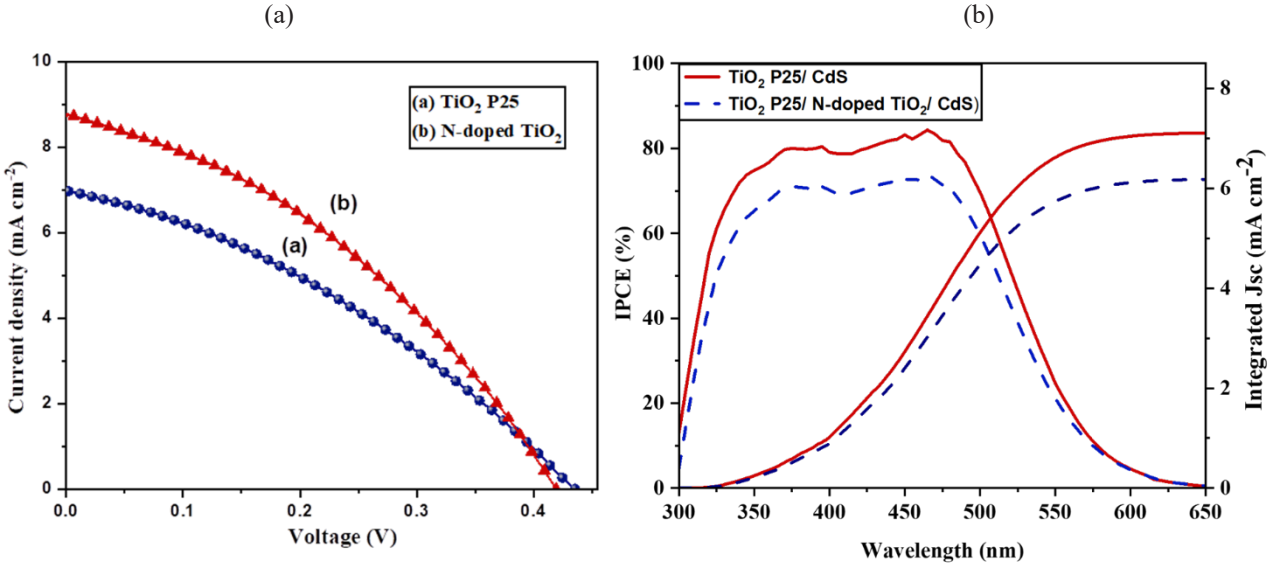

Figure 6: (a) Current density - Voltage (J-V) characteristics of CdS QDSSCs with (a) TiO_2 P25 and (b) TiO_2 P25/ N-doped TiO_2 photoanodes and, (b) IPCE spectra and integrated current density curves of CdS QDSSCs with TiO_2 P25 and TiO_2 P25/ N-doped TiO_2 photoanodes.

Table 1: Photovoltaic parameters of CdS QDSSCs assembled with TiO_2 P25 and TiO_2 P25/ N-doped TiO_2 photoanodes.

QDSSC	Photoanode	Integrated *J*sc (mA cm^{-2})	*J*sc (mA cm-2)	*V*oc (mV)	FF (%)	Efficiency (%)
S_1	TiO_2 P25/ CdS	6.04	6.81 ± 0.13	435.0 ± 1.5	35.16 ± 0.70	1.04 ± 0.01
S_2	TiO_2 P25/ N-doped TiO_2/ CdS	7.11	8.61 ± 0.11	420.2 ± 2.0	36.74 ± 0.37	1.35 ± 0.02

Table 2: EIS parameters of CdS QDSSCs with TiO_2 P25 and TiO_2 P25/ N-doped TiO_2 photoanodes.

QDSSC	Photoanode	*R*s (Ω)	R_1ct (Ω)	R_2ct (Ω)
S_1	TiO_2 P25/ CdS	7.35	30.5	129.0
S_2	TiO_2 P25/ N-doped TiO_2/ CdS	7.22	26.1	95.8

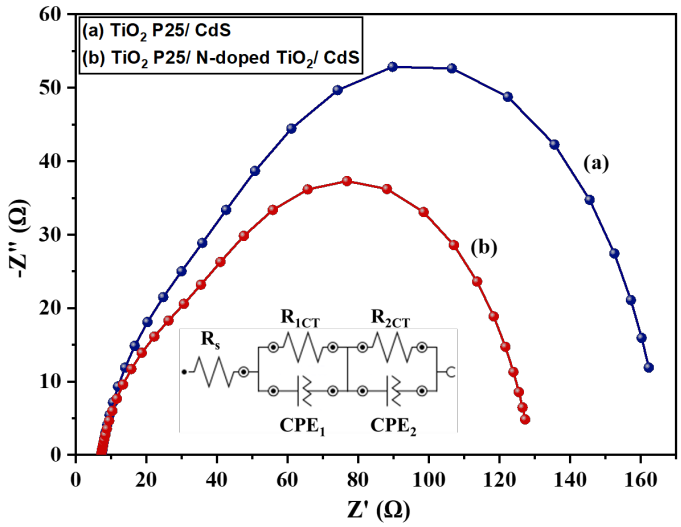

Figure 7: EIS Nyquist plots of CdS QDSSCs with TiO_2 P25 and TiO_2 P25/ N-doped TiO_2 photoanodes.

in N-doped TiO_2 photoanode and a higher R_2ct value is expected. However, higher photocurrent generation in the photoanode dominate over these negative effects resulting in an improved R_2ct (Dissanayake *et al*., 2017).

CONCLUSION

In this study, a triple-layer photoanode was successfully constructed with layer-by-layer fabrication of TiO_2 P90 compact layer, TiO_2 P25 layer and N-doped TiO_2 layer. N-doped TiO_2 nanocrystals, which belongs to the anatase crystal structure, were synthesized using a wet chemical method and thermally treating at 450 °C. The incorporation of the N-doped TiO_2 layer in CdS QDSSCs enhanced overall power conversion efficiency by 29.81 % compared to the addition of a TiO_2 P25 layer. Similarly, due to efficient photocurrent generation in the photoanode., charge transfer resistance at the photoanode/ electrolyte interface has reduced by 25.7 % with the incorporation of N-doped TiO_2 layer.

DECLARATION OF CONFLICT OF INTEREST

The authors declare no conflict of interests.

ACKNOWLEDGEMENT

This research was supported by the research grant (DOR9-2019) awarded by the Accelerating Higher Education Expansion and Development (AHEAD) Operation of the Ministry of Higher Education funded by the World Bank.

REFERENCES

Abeles, F. (1972). *Optical properties of solids. Ed. by F. Abeles*. North-Holland Pub. Co.; American Elsevier.

Baur, W. H. and Khan, A.A. (1971). Rutile-type compounds. IV. SiO_2, GeO_2 and a comparison with other rutile-type structures. *Acta Crystallographica Section B Structural Crystallography and Crystal Chemistry*, **27**(11): 2133-2139. DOI: https://doi.org/10.1107/s0567740871005466.

Borovaya, M.N., Naumenko, A.P., Matvieieva, N.A., Blume, Y.B. and Yemets, A.I. (2014). Biosynthesis of luminescent CdS quantum dots using plant hairy root culture. *Nanoscale Research Letters*, **9**(1): 1-7. DOI: https://doi.org/10.1186/1556-276X-9-686.

Dissanayake, M.A.K.L., Jaseetharan, T., Senadeera,

G.K.R. and Kumari, J.M.K.W. (2020). Efficiency enhancement in PbS/CdS quantum dot-sensitized solar cells by plasmonic Ag nanoparticles. *Journal of Solid State Electrochemistry*, **24**(2): 283-292. DOI: https://doi.org/10.1007/s10008-019-04420-4.

Dissanayake, M.A.K.L., Kumari, J.M.K.W., Senadeera, G.K.R. and Anwar, H. (2021a). Low cost, platinum free counter electrode with reduced graphene oxide and polyaniline embedded SnO_2 for efficient dye sensitized solar cells. *Solar Energy*, *230*(October), 151-165. DOI: https://doi.org/10.1016/j.solener.2021.10.022.

Dissanayake, M.A.K.L., Kumari, J.M.K.W., Senadeera, G. K. R., Jaseetharan, T., Weerasinghe, J. and Anwar, H. (2021b). A low-cost, vein graphite/tin oxide nanoparticles based composite counter electrode for efficient dye-sensitized solar cells. *Materials Science and Engineering B: Solid-State Materials for Advanced Technology*, **273**(August): 115440. DOI: https://doi.org/10.1016/j.mseb.2021.115440.

Dissanayake, M.A.K.L., Kumari, J.M.K.W., Senadeera, G.K.R., Thotawatthage, C.A., Mellander, B.E. and Albinsson, I. (2017). A novel multilayered photoelectrode with nitrogen-doped TiO_2 for efficiency enhancement in dye sensitized solar cells. *Journal of Photochemistry and Photobiology A: Chemistry*, **349**: 63-72. DOI: https://doi.org/10.1016/j.jphotochem.2017.08.067

Garlisi, C., Lai, C.Y., George, L., Chiesa, M. and Palmisano, G. (2018). Relating Photoelectrochemistry and Wettability of Sputtered Cu- and N-Doped TiO_2 Thin Films via an Integrated Approach. *Journal of Physical Chemistry C*, **122**(23): 12369-12376. DOI: https://doi.org/10.1021/acs.jpcc.8b03650.

Gelderman, K., Lee, L. and Donne, S.W. (2007). Flat-band potential of a semiconductor: Using the Mott-Schottky equation. *Journal of Chemical Education*, **84**(4): 685-688. DOI: https://doi.org/10.1021/ed084p685.

Guo, W., Shen, Y., Boschloo, G., Hagfeldt, A. and Ma, T. (2011). Influence of nitrogen dopants on N-doped TiO_2 electrodes and their applications in dye-sensitized solar cells. *Electrochimica Acta*, **56**(12): 4611-4617. DOI: https://doi.org/10.1016/j.electacta.2011.02.091.

Guo, W., Shen, Y., Wu, L., Gao, Y. and Ma, T. (2011). Effect of N dopant amount on the performance of dye-sensitized solar cells based on N-Doped TiO_2 electrodes. *Journal of Physical Chemistry C*, **115**(43): 21494-21499. DOI: https://doi.org/10.1021/jp2057496.

Horn, M., Schwerdtfeger, C. F. and Meagher, E. P. (1972). Refinement of the structure of anatase at several temperatures. *Zeitschrift Fur Kristallographie - New Crystal Structures*, **136**(3-4): 273-281. DOI: https://doi.org/10.1524/zkri.1972.136.3-4.273.

Khan, T.T., Rafiqul Bari, G.A.K.M., Kang, H.J., Lee, T.G., Park, J.W., Hwang, H.J., Hossain, S.M., Mun, J.S., Suzuki, N., Fujishima, A., Kim, J.H., Shon, H.K. and Jun, Y.S. (2021). Synthesis of N-doped TiO_2 for efficient photocatalytic degradation of atmospheric NOx. *Catalysts*, **11**(1): 1-13. DOI: https://doi.org/10.3390/catal11010109.

Kubelka, P. and Munk, F. (1931). An article on optics of paint layers. *Z. Tech. Phys.*, **12**(1930): 593-601.

Kumar, P.N., Das, A. and Deepa, M. (2020). Nitrogen doping of TiO_2 and annealing treatment of photoanode for enhanced solar cell performance. *Journal of Alloys and Compounds*, **832**: 154880. DOI: https://doi.org/10.1016/j.jallcom.2020.154880.

Kushwaha, R., Chauhan, R., Srivastava, P. and Bahadur, L. (2015). Synthesis and characterization of nitrogen-doped TiO_2 samples and their application as thin film electrodes in dye-sensitized solar cells. *Journal of Solid State Electrochemistry*, **19**(2): 507-517. DOI: https://doi.org/10.1007/s10008-014-2623-8.

La Mantia, F., Habazaki, H., Santamaria, M. and Di Quarto, F. (2010). A critical assessment of the Mott-Schottky analysis for the characterisation of passive film-electrolyte junctions. *Russian Journal of Electrochemistry*, **46**(11): 1306-1322. DOI: https://doi.org/10.1134/S102319351011011X.

Li, C., Wu, H., Zhu, L., Xiao, J., Luo, Y., Li, D., Meng, Q., Li, C., Wu, H., Zhu, L., Xiao, J., Luo, Y. and Li, D. (2014). Study on negative incident photon-to-electron conversion efficiency of quantum dot- sensitized solar cells Study on negative incident photon-to-electron conversion efficiency of quantum dot-sensitized solar cells. *023103*. DOI: https://doi.org/10.1063/1.4865115.

Li, D., Fu, Z., Han, Q., Lin, C.H., Gao, S., Xiong, Y. and Wen, T.C. (2020). A Ternary-Mixture-Based Counter Electrode for Quantum-Dot-Sensitized Solar Cells. *ACS Applied Energy Materials*, **3**(7): 7121-7128. DOI: https://doi.org/10.1021/acsaem.0c01177.

López-Luke, T., Wolcott, A., Xu, L.P., Chen, S., Wen, Z., Li, J., De La Rosa, E. and Zhang, J.Z. (2008). Nitrogen-doped and CdSe quantum-dot-sensitized nanocrystalline TiO_2 films for solar energy conversion applications. *Journal of Physical Chemistry C*, **112**(4): 1282-1292. DOI: https://doi.org/10.1021/jp077345p.

Patil, G.E., Kajale, D.D., Gaikwad, V.B. and Jain, G.H. (2012). Preparation and characterization of SnO_2 nanoparticles by hydrothermal route. International Nano Letters, **2**(1). https://doi.org/10.1186/2228-5326-2-17.

Kusumawardani, C. and Narsito, I.K. (2010). Chemically Synthesized Mesoporous Nitrogen-Doped TiO_2 and its Application to High Efficiency Dye- Sensitized Solar Cells. Thammasat International Journal of Science and Technology, **15**(4).

Qiu, X. and Burda, C. (2007). Chemically synthesized nitrogen-doped metal oxide nanoparticles. *Chemical Physics*, **339**(1-3): 1-10. DOI: https://doi.org/10.1016/j.chemphys.2007.06.039.

SATO, N. (1990). Electrocthemistry of Semiconductors. *Tetsu-to-Hagane*, **76**(9):1423-1436. DOI: https://doi.org/10.2355/tetsutohagane1955.76.9_1423.

Scherrer, P. (1918). Nachr Ges wiss goettingen. Math. Phys., **2:** 98-100.

Shu, T., Xiang, P., Zhou, Z. M., Wang, H., Liu, G.H., Han, H.W. and Zhao, Y. Di. (2012). Mesoscopic nitrogen-doped TiO_2 spheres for quantum dot-sensitized solar cells. *Electrochimica Acta*, **68**: 166-171. DOI: https://doi.org/10.1016/j.electacta.2012.02.068.

Shu, T., Zhou, Z., Wang, H., Liu, G., Xiang, P. and Rong, Y. (2011). Efficient CdPbS Quantum Dots-Sensitized

TiO_2 Photoelectrodes for Solar Cell Efficient CdPbS Quantum Dots-Sensitized TiO2 Photoelectrodes for Solar Cell Applications. *Journal of Nanoscience and Nanotechnology,* **11**(11): 9645-9649. https://doi.org/10.1166/jnn.2011.5325.

Spurr, R.A. and Myers, H. (1957). *Quantitative Analysis of Anatase-Rutile Mixtures with an X-Ray Diffractometer*.

Tayade, R.J. and Gandhi, V. (2018). Photocatalytic nanomaterials for environmental applications. *Materials Research Forum LLC*.

Thenmozhi, C., Manivannan, V., Kumar, E. and Veera Rethina Murugan, S. (2015). Synthesis and characterization of SnO_2 nanoparticles by microwave - assisted solution method. *International Journal of Current Research,* **7**(11): 23162-23166.

Tian, H., Hu, L., Zhang, C., Liu, W., Huang, Y., Mo, L., Guo, L., Sheng, J. and Dai, S. (2010). Retarded charge recombination in dye-sensitized nitrogen-doped TiO_2 solar cells. *Journal of Physical Chemistry C*, **114**(3): 1627-1632. DOI: https://doi.org/10.1021/jp9103646.

Umair, K., Dissanayake, M.A.K.L. and Senadeera, G.K. R. (2021). Efficiency enhancement in SnO_2 based dye-sensitized solar cells by incorporating plasmonic gold nanoparticles. *Ceylon Journal of Science*, **50**(5): 341. DOI: https://doi.org/10.4038/cjs.v50i5.7923.

Zhang, J., Sun, Q., Zheng, J., Zhang, X., Cui, Y., Wang, P., Li, W. and Zhu, Y. (2011). The characterization of nitrogen doped TiO_2 photoanodes and its application in the dye sensitized solar cells. *Journal of Renewable and Sustainable Energy*, **3**(3). DOI: https://doi.org/10.1063/1.3599840.

Zhang, Z.L., Li, J. F., Wang, X.L., Qin, J.Q., Shi, W.J., Liu, Y.F., Gao, H.P. and Mao, Y.L. (2017). Enhancement of Perovskite Solar Cells Efficiency using N-Doped TiO_2 Nanorod Arrays as Electron Transfer Layer. *Nanoscale Research Letters,* **12**(1): 1-7.DOI: https://doi.org/10.1186/s11671-016-1811-0.